Journal of Nuclear Materials 393 (2009) 282–291

Contents lists available at ScienceDirect

Journal of Nuclear Materials

journal homepage: www.elsevier.com/locate/jnucmat

Low temperature age hardening in U–13 at.% Nb: An assessment of chemical redistribution mechanisms

A.J. Clarke [a], R.D. Field [a], R.E. Hackenberg [a,*], D.J. Thoma [a], D.W. Brown [a], D.F. Teter [a], M.K. Miller [b], K.F. Russell [b], D.V. Edmonds [c], G. Beverini [c]

[a] Materials Science and Technology Division, Mail Stop G770, Los Alamos National Laboratory, Los Alamos, NM 87545, USA
[b] Materials Science and Technology Division, Microscopy, Mail Stop 6136, Oak Ridge National Laboratory, Oak Ridge, TN 37831, USA
[c] School of Process, Environmental and Materials Engineering, University of Leeds, Leeds LS2 9JT, United Kingdom

ARTICLE INFO

Article history:
Received 1 November 2008
Accepted 15 June 2009

ABSTRACT

Low temperature aging (<350 °C) of U–13 at.% Nb martensite results in increased strength levels accompanied by significant ductility loss. To determine the decomposition mechanism(s) responsible for these mechanical property changes, atom probe tomography was used to examine the niobium and impurity distributions after aging at 200 or 300 °C for times ranging from 2 h to 70 days. No patterns of niobium or impurity atoms were observed that would indicate segregation to the martensitic twin interfaces, making this hardening mechanism unlikely. Phase separation into roughly equiaxed regions of high and low niobium concentration was clearly observed after aging at 300 °C for 70 days. However, only subtle niobium concentration changes were observed after aging at 200 °C relative to the as-quenched condition, indicating that conventional phase separation is an unlikely explanation for the dramatic mechanical property changes at 200 °C. Therefore, consideration of aging mechanisms other than segregation and phase separation may be warranted.

1. Introduction

Uranium can be alloyed with transition metal elements such as Ti, V, Cr, Zr, Nb, and Mo to improve the physical, mechanical, and corrosion properties relative to unalloyed uranium [1]. Such alloys are suitable for defense and other applications where high density, tailored strength/ductility combinations, corrosion resistance, and formability are desirable. Uranium alloys can exhibit age–hardening responses owing to the considerable solubility of these transition metal elements in the body centered cubic (bcc) γ phase at high temperatures and their virtual insolubility in the lower temperature phases. The low-solubility phases observed at lower temperatures include a variety of metastable phases, in addition to the orthorhombic α-U phase that is the equilibrium ambient-temperature matrix phase in unalloyed uranium and in many of its alloys. These alloys exhibit complex phase transformation pathways when starting from single-phase γ microstructure.

U–Nb alloys with compositions near 14% Nb[1] exhibit outstanding corrosion resistance when the niobium solute is uniformly distributed in the microstructure [1,2]. Such a microstructure is attained when the high temperature γ phase is rapidly cooled to room temperature, resulting in niobium-supersaturated metastable phases, including the α′, α″, and γ^0 martensite phases. The α′ phase is martensitically formed orthorhombic α, whereas the α″ and γ^0 phases are monoclinically distorted α′ and tetragonally distorted γ, respectively [3–8]. At ambient temperature, the α′ phase exists over the concentration range 0–8% Nb, the α″ phase over the 9–15% Nb range, and the γ^0 phase over the 16–20% Nb range [3]. At >20% Nb, the metastable (niobium-supersaturated) γ phase is retained. For the case of U–14% Nb (a highly hardenable uranium alloy), a completely α″ martensite microstructure is realized for quench rates greater than 20 K/s [2]. This microstructure exhibits low yield strength (100–200 MPa), high ductility (~30% tensile elongation) and formability, and the shape-memory effect (SME), in addition to outstanding corrosion resistance [2,5,9–14].

Below the 647 °C monotectoid isotherm, martensitic microstructures are metastable with respect to the equilibrium two-phase mixture of $\alpha + \gamma_2$, shown on the phase diagram in Fig. 1 [15]. The orthorhombic α phase is nearly pure U, and the bcc γ_2 phase contains ~75% Nb. Many of the desirable properties of as-quenched U–14% Nb will degrade as a result of age–hardening reactions that decompose the niobium-supersaturated α″ during insufficiently rapid cooling (0.2–20 K/s) [2] or isothermal aging treatments.

Jackson identified two principal kinetic modes of aging that correspond to two separate *C*-curves on the *T*–*T*–*T* diagram for U–13% Nb [16]. Similar decomposition reactions take place at a given

* Corresponding author.
E-mail address: roberth@lanl.gov (R.E. Hackenberg).

[1] Compositions of bulk alloys and phases are reported in at.%, unless otherwise indicated.

0022-3115/$ - see front matter © 2009 Elsevier B.V. All rights reserved.
doi:10.1016/j.jnucmat.2009.06.025

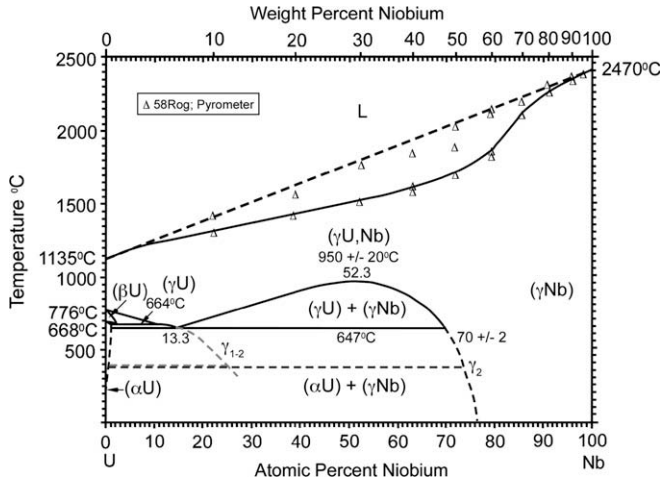

Fig. 1. The U–Nb equilibrium phase diagram, adapted from Koike et al. [15].

temperature regardless of whether the thermal path is direct isothermal or cooling transformation from the stable γ phase region, or decomposition of the α″ phase upon quenching and subsequent aging. The higher temperature *C*-curve, spanning 300–647 °C with a 550 °C nose, corresponds to the cellular (discontinuous) precipitation of a lamellar $\alpha + \gamma_{1-2}$ product [2,16–22]. The γ_{1-2} phase is bcc with an intermediate composition defined by a metastable extension of the equilibrium monotectoid solvus (14–35% Nb); it evolves toward the equilibrium γ_2 composition (~75% Nb) with concomitant formation of additional α [2,16,17,20]. The resulting microstructures are undesirable from a corrosion and ductility standpoint, and are only marginally better than unalloyed uranium [21].

The reaction(s) corresponding to the lower *C*-curve [16], with a nose at 400 °C, results in considerable strengthening and ductility loss [2,18,19,21–25], with only marginal decrements in corrosion resistance [2]. The specific aging mechanism(s) for this low-temperature decomposition mode are unclear, though many U–Nb aging studies have proposed some variant of diffusional niobium redistribution. Mechanisms that have been considered include classical nucleation-and-growth (N&G) [16], spinodal decomposition [2,16,26,27], chemical ordering [26,27], and precursors to phase separation[2] involving niobium diffusion, such as clustering and segregation to defects, particularly α″ twin boundaries [16,21,28]. Niobium (or impurity) segregation to existing twin boundaries is a potentially potent strengthening mechanism in view of the high twin mobility in as-quenched U–14% Nb. Preferential segregation (or precipitation) could impede twin boundary motion in response to an applied stress, thereby resulting in strengthening [21,28].

Diffraction and dilatometry experiments provide indirect evidence that niobium redistribution occurs during low temperature (⩽300 °C) U–Nb martensite aging [16,24,25,29,30]. Kinetic analyses based upon mechanical property changes resulted in activation energies (*Q*) of 121–138 kJ/mol in U–13% Nb [24] and 117 kJ/mol in U–11% Nb [21]; these values are close to the Q_{diff} = 138 kJ/mol measured for niobium volume diffusion in γ-U[3] [31]. These diffraction and kinetic results suggest phase separation governed by niobium volume diffusion, though conclusions regarding a specific mechanism of phase separation are tentative since these methods are indirect. Attempts to directly image the separating phases by transmission electron microscopy (TEM) were equivocal and inconclusive in view of the seemingly fine scale (⩽3 nm) of the aging-related microstructural changes [2,22,24–27,29].

Atom probe tomography (APT) is well-suited to discriminate between the proposed aging mechanisms, since niobium and impurity distributions can be resolved at the atomic level. A 1D atom probe study on U–14% Nb aged at 300, 400, and 450 °C was performed by Beverini and Edmonds [22]. Strengthening in U–14% Nb after aging at or above 400 °C was attributed to classical nucleation-and-growth of a niobium-enriched phase. Examination of a specimen aged at 300 °C for 16 h showed concentration fluctuations on the order of 3 nm, which was corroborated by TEM evidence that showed aligned contrast modulations with a similar length scale. On this basis, the possibility that spinodal decomposition may operate at <400 °C was proposed. Segregation of niobium or impurity atoms to α″ twin interfaces was not evident.

The inconclusiveness of recent diffraction and electron microscopy studies [24,25,30] have prompted re-examination of U–13% Nb with APT, to provide insight regarding the specific mechanism(s) responsible for age–hardening in this alloy. Such a study is timely, given recent advances in atom probe instrumentation [32], which enables the ability to resolve atom positions in 3D, and allows for the collection of more total atoms per specimen at significantly faster rates. Enhanced data returns will provide higher-fidelity snapshots of local chemical environments in aged microstructures, allowing for critical assessments of proposed aging mechanisms premised on chemical redistribution.

2. Experimental

2.1. Material and mechanical properties

A U–13% Nb alloy was vacuum induction melted and cast into 0.5″ thick plate, hot rolled to 50% reduction over eight rolling passes at 850 °C, homogenized at 1000 °C for 6 h under dynamic vacuum, and then furnace cooled. Chemical analysis by inductively coupled plasma mass spectroscopy (ICP-MS) showed the average niobium content was 13.2 at.% Nb. Sampling of the plate indicated the variation in niobium content to be ±1.2 at.% from ICP-MS and ±0.4 at.% from electron microprobe analysis. The bulk levels of the minor elements are listed in Table 1. Silicon was observed but not quantified. More details of the synthesis and characterization can be found in [33].

Table 1
Concentrations of minor elements in the U–13.2 at.% Nb alloy [33]. The values in wppm were the output of the instrument; values in the other units were derived. The metallic element values were from ICP-MS; H, C, N and O were determined from dedicated analyzers.

Element	wt.%	wppm	appm	at.%
H	0.0002	1.5	324	0.0324
C	0.0150	150	2722	0.2722
N	0.0020	20	311	0.0311
O	0.0041	41	559	0.0559
Mg	0.0003	3	27	0.0027
Al	0.0043	43	347	0.0347
Ti	0.0009	9	41	0.0041
V	0.0008	8	34	0.0034
Cr	<0.0004	<4	<17	<0.0017
Mn	0.0008	8	32	0.0032
Fe	0.0047	47	183	0.0183
Ni	0.0012	12	45	0.0045
Zr	0.0011	11	26	0.0026
Mo	0.0001	1	2	0.0002
Ta	0.0050	50	60	0.0060
W	0.0007	7	8	0.0008

[2] In this context, "phase separation" is defined broadly as any mechanism resulting in the formation of additional phases, including spinodal and N&G mechanisms.

[3] When heated to 200–300 °C, U–13% Nb martensitically reverts to the tetragonal γ^0 phase and undergoes the initial increment of aging in this phase [30]. The activation energy Q_{diff} for Nb volume diffusion is expected to be similar for γ^0 and γ in view of their structural similarities.

Cylindrical tensile specimens, with an initial gauge diameter of 2.54 mm and an initial total gauge length of 17.8 mm, and coupons for hardness measurements were prepared. These specimens were solution heat treated at 800 °C for 30 min in an evacuated-and-Ar-backfilled quartz capsule that was gettered with Ti. The capsule was shattered during water quenching, producing the as-quenched (AQ) niobium-supersaturated α″ martensite microstructure. A few specimens were tested in the AQ condition; the remainder of the specimens were re-encapsulated and aged at 200 or 300 °C in air furnaces for times of 100 min (~2 h), 1000 min (~16 h), 10,000 min (~7 days), or 100,000 min (~70 days), followed by air cooling. The solutionizing and aging treatments were performed *after* the final machining to avoid interference from apparent strengthening attributable to machining damage [24]. Quasistatic tensile testing was performed at room temperature at a nominal strain rate of 0.001 s^{-1} using a screw-driven load frame. Displacement data were recorded with an extensometer. Vickers microhardness measurements (500 g load) were performed on the AQ and aged coupons.

2.2. Atom probe tomography and field ion microscopy

Electrodischarge machining (EDM) was used to cut oversized atom probe specimen blanks that were then mechanically ground to nominal dimensions of $\sim 0.25 \times \sim 0.25 \times \sim 10\ mm^3$ to remove the EDM recast layer. Solutionizing and aging was performed using the procedure described above. The aging times used were 120 min (2 h) and 960 min (16 h), in addition to 10,000 and 100,000 min. These aging times were similar to those used for the tensile and hardness specimens. The atom probe specimen blanks were electropolished into sharp needles using a two-stage double layer technique, in combination with micropolishing that utilizes a wire loop with a drop of suspended electrolyte [32]. The respective electrolytes and voltages used were 25% perchloric acid (72%) in glacial acetic acid at 18 V DC and 2% perchloric acid in 2-butoxyethanol at 16 V DC [32]. The electropolished, tapered needle specimens were immediately stored and transported under methanol to minimize oxidation prior to analysis.

The APT analysis was done with a local electrode atom probe (LEAP®)[4] instrument. The specimen temperature was 60 K. A pulse fraction of 20% and pulse repetition rate of 200 kHz were used. Two or more replicate specimens were run for each aging condition. The number of atoms collected and identified for each APT run was on the order of 10^7. Field ion microscopy (FIM) was performed with a Kindbrisk 3D atom probe on a specimen aged 70 days at 300 °C, with the goal of observing niobium at locations such as at α″ twin boundaries.

Analysis of the APT data was done with a combination of Imago Scientific Instruments IVAS, Kindbrisk Posap and Oak Ridge National Laboratory (ORNL) software. The atomic co-ordinates and mass-to-charge state of all detected atoms within the analyzed volume of each tapered needle specimen were determined. Isoconcentration contour surfaces were generated in which areas with a niobium concentration greater than a given threshold (25%, for example) were enclosed by the surface. Concentration profiles through the volume were also generated using a $4 \times 4\ nm^2$ cross-section box that was run in a specified direction (defined in relation to the tapered cylinder, not any particular crystallographic direction; no attempt was made to determine the crystallographic orientation of the APT specimens via TEM or any other method). Five-point moving average smoothing and a 0.25 nm bin size was employed for all of the concentration profiles presented.

For a particular atom-probe data set, the average niobium concentration was determined from a frequency distribution (histogram), where the atoms in the selected volume were divided into blocks containing a fixed number of atoms; 100 atom blocks were used for the data presented here [32]. A binomial distribution was generated for the estimated local average niobium content in the APT dataset. For the AQ condition, a correspondence between the experimental data and the binomial profile is anticipated. An experimental aged-condition profile that is sharper than the binomial (or the actual AQ profile) indicates a tendency toward chemical ordering, whereas an experimental profile that is broader indicates a tendency toward solute clustering or new-phase formation.

The experimentally observed frequency distribution profiles were analyzed under the framework established by Langer, Baron, and Miller (LBM) [32,34,35]. This framework decomposes the total profile into a pair of best-fit Gaussian distributions centered at μ_1 and μ_2, each with a half-width of σ. The μ_1 and μ_2 parameters can be estimated from the solute concentrations (parameters b_1 and b_2) relative to the mean solute concentration (c_0), using the expressions $\mu_1 = c_0 - b_2$ and $\mu_2 = c_0 + b_1$. The maximum likelihood method is used to fit the parameters b_1, b_2, and σ [32]. In essence, μ_1 and μ_2 represent the average compositions of the phases or solute clusters that have evolved out of an initially single-phase supersaturated solid solution. The peak separation $\Delta c = |\mu_2 - \mu_1|$ is a measure of the extent (amplitude) of decomposition. Although the LBM method was originally developed to treat non-linear spinodal decomposition, its applicability is not restricted to the spinodal region, making it useful to the present study where the specific aging mechanism (spinodal, N&G, clustering, segregation, etc.) is not known *a priori*.

3D autocorrelation functions were also generated from the data sets to gain insight into the spacing and size of niobium clusters. The results were inconclusive, however.

3. Results

3.1. Mechanical properties

The engineering stress–strain curves obtained for the AQ condition and after aging at 200 or 300 °C are shown in Fig. 2a. The stress–strain response of the α″ martensite in the AQ and low-to-intermediate aged conditions is two-stage, exhibiting two apparent yield points. The shape of the stress–strain curve within the low strain regime is attributed to SME twinning and twin motion [5,9–11], whereas straining past the second yield point (at ~7% strain) is generally associated with irreversible deformation such as slip [5,10,12–14]. Significant changes in stress–strain response are observed after low temperature aging, which is evident in the stress–strain curves of Fig. 2a after aging at 200 or 300 °C. Substantial increases in the first yield point and decreases in elongation are observed as aging time and temperature increase. The most severe ages examined, 70 days at 200 and 300 °C, exhibited almost no ductility.

The hardness response after 200 or 300 °C aging for times up to 70 days is shown in Fig. 2b; the increasing hardness with increasing time and temperature is consistent with the stress–strain behavior. Peak hardness values are not evident from the data presented in Fig. 2b, though in this context it is important to note that no signs of overaging were found. The cellular (lamellar) decomposition products, the classical signature of overaging [21], were not observed by light optical metallography in any of the aging conditions examined by APT.

3.2. Atom probe tomography and field ion microscopy: general

Evidence of interstitial impurity atoms – C, N, or O – above the background level was not obtained in any of the APT analyses. This

[4] LEAP is a registered trademark of Imago Scientific Instruments, Madison, WI.

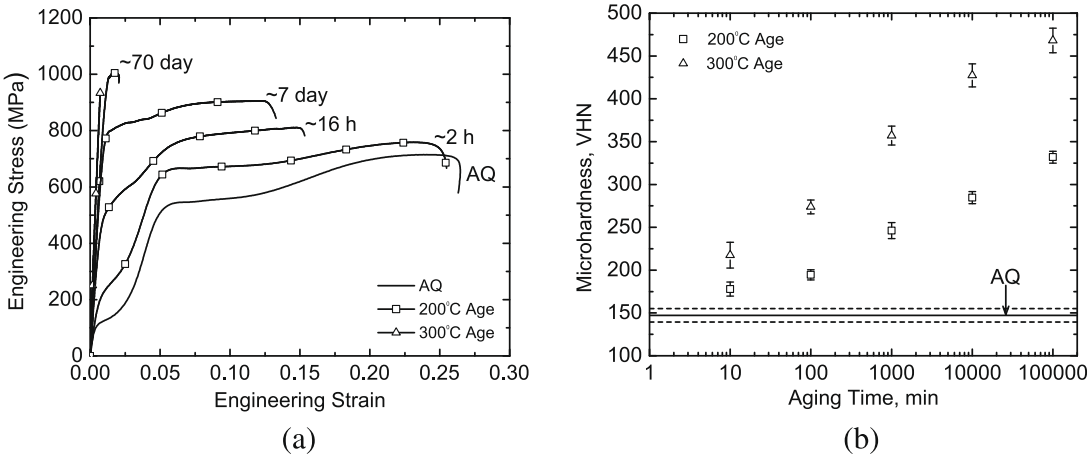

Fig. 2. Representative (a) tensile curves and (b) hardness values obtained after low temperature aging of U–13% Nb. The solid and dashed lines in (b) indicate the average and standard deviation of the AQ hardness, respectively. All the aging conditions shown in (a) were subjected to APT interrogation, including the 70-day ages at both 200 and 300 °C that exhibit virtually no ductility.

is not surprising, given their propensity to form carbide, nitride, or oxide inclusions of sufficiently large size and spacing in the bulk material to avoid a realistic probability of their being encountered in the sampled volumes of the APT specimens. Some (~1 at.%) hydrogen was detected. However, it is difficult to establish whether the hydrogen is from the specimen or from the background level of hydrogen in the ultrahigh vacuum system. Beverini and Edmonds reported low (or nonexistent) amounts of C and O in their analyses [22]. They did observe hydrogen, but were unable to determine if it had segregated to α″ twin interfaces.

Atom maps generated as thin (2 or 4 nm thick) slices through the analyzed 3D volume showed what appeared to be random distributions of both niobium and the major substitutional impurity atoms (Al, Si, and Fe). Although the specific locations of the α″ twin boundaries in any given APT specimen were not determined, at least 3 or 4 twin boundaries are expected to cut through an average APT specimen, given that the analyzed volume of a typical specimen is ~200 nm tall and ~40 nm in diameter, while typical fine twin spacings in U–13% Nb are 20–50 nm [5]. Thus, significant segregation to twin boundaries, if present, should be observable in the atom maps. Patterning, especially that indicative of niobium or impurity atom enrichment or depletion to twin boundaries, was observed in neither the AQ nor in any of the aged conditions.

Contrast specific to prior γ grain boundaries, α″ twin boundaries, niobium-rich regions, or other pertinent features could not be discerned by field ion microscopy on the most severely aged specimen (300 °C, 70 days), where such features would presumably be the most noticeable. This lack of contrast is similar to that reported in an earlier FIM study [22].

3.3. Atom probe tomography: as-quenched (AQ) condition

A niobium-concentration profile for the AQ condition is shown in Fig. 3a. Some niobium concentration variations are observed above and below 13.2% Nb, the niobium level indicated from bulk chemical analysis. This variation is better quantified by the experimental frequency distribution (solid line) in Fig. 3b. These data were fitted to the LBM model as described previously; the experimental distributions and LBM fit match each other so closely that they are indistinguishable in the figure. The experimental profile is slightly broader and has a lower peak amplitude compared to the binomial distribution; the latter was evaluated at the local average niobium concentration in the specimen determined from the APT data (14.7% Nb). This difference suggests that some nonrandomness may exist in the AQ condition, which might be an indication of clustering. Beverini and Edmonds also observed similar nonrandom behavior in the concentration histogram of the AQ

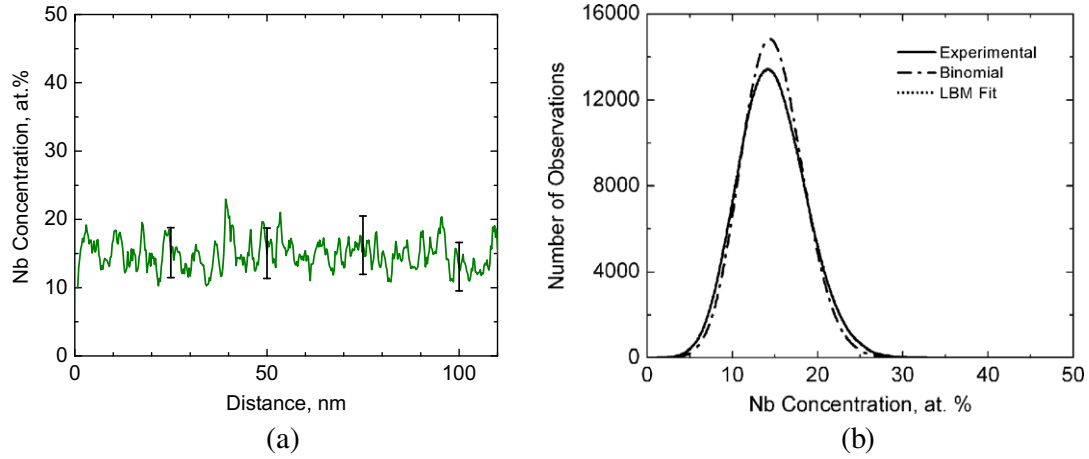

Fig. 3. APT results for the AQ condition. (a) Niobium concentration profile; the ±1 standard error is shown every 25 nm. (b) Experimental, LBM-fit, and binomial frequency distributions of the niobium concentrations; note that the experimental and LBM curves lie on top of one another. The LBM-fit niobium concentrations of the hypothetical coexisting phases were the average (14.7) + 1.8 and −1.2% Nb.

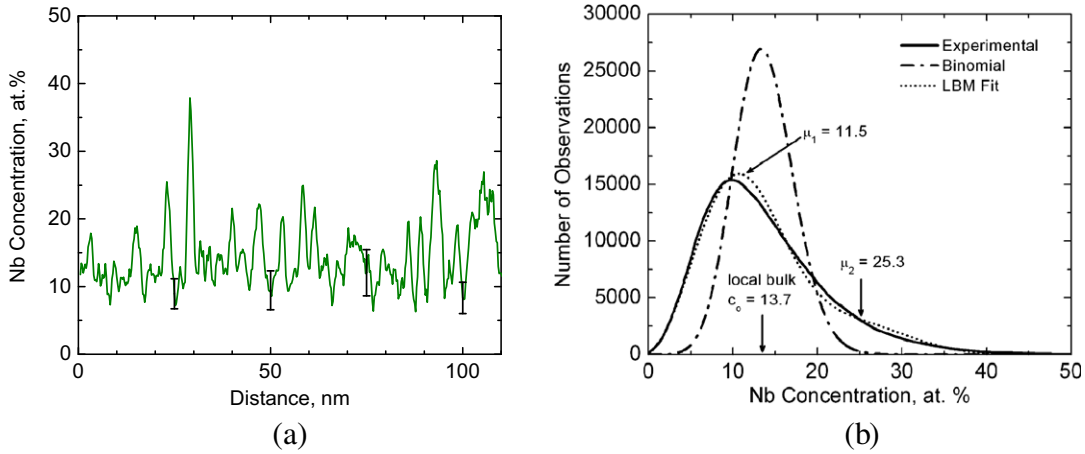

Fig. 4. APT results for the 300 °C, 70 days aged condition. (a) Niobium concentration profile; the ±1 standard error is shown every 25 nm. (b) Experimental, LBM-fit, and binomial frequency distributions of the niobium concentrations. The LBM-fit niobium concentrations of the hypothetical coexisting phases were the average (13.7) + 11.6 and −2.2% Nb, which are indicated on the figure along with the local bulk concentration used to calculate the binomial distribution.

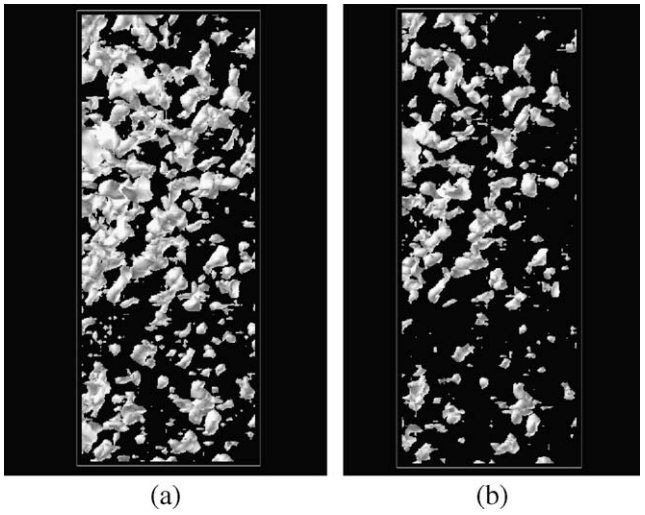

Fig. 5. Niobium isoconcentration surfaces obtained for the 300 °C, 70 days aged condition. (a) 30% surface. (b) 35% surface. The box size is 40 nm wide × 40 nm deep × 100 nm tall.

condition. Autocorrelation analysis failed to reveal any periodicity to the nonrandomness. The origin of the nonrandomness is unclear, but in any event is small in magnitude.

3.4. Atom probe tomography: quenched and aged at 300 °C

The 300 °C, 70 days aging condition resulted in the highest strength and lowest ductility of all the aging conditions examined (Fig. 2). A representative niobium concentration profile and frequency distribution are shown together in Fig. 4. The niobium concentration profile differs substantially from that obtained for the AQ condition, as niobium-enriched and depleted regions are noticeably present, indicating clustering or phase separation. A characteristic wavelength of 6–8 nm is evident. The experimental frequency distribution is significantly more asymmetrical and broader than the binomial distribution, again consistent with clustering or phase separation. The concentrations of the coexisting clusters or phases determined from the LBM method are 11.5% and 25.3% Nb. Isoconcentration surfaces for the 30% and 35% Nb levels are shown in Fig. 5, which further highlight the niobium enriched regions within the microstructure for this condition. These enriched regions appear more or less equiaxed in shape.

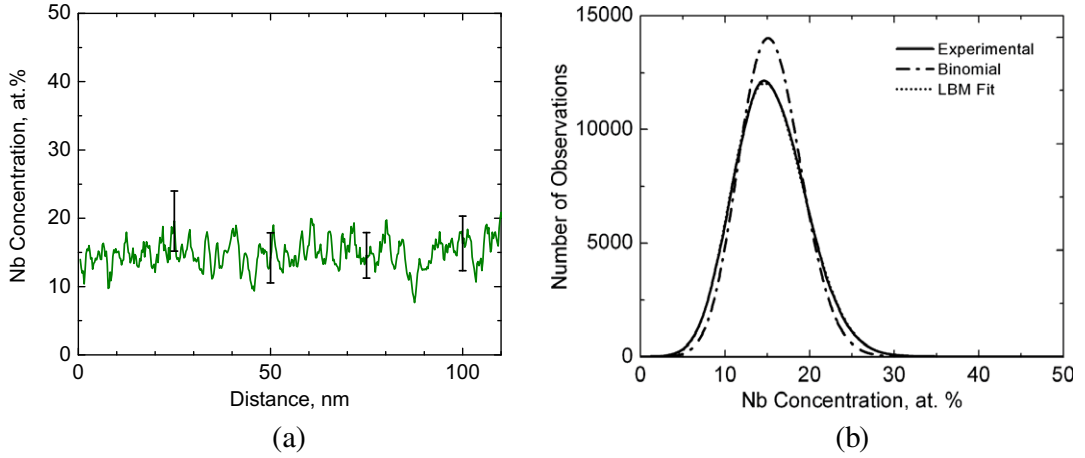

Fig. 6. APT results for the 200 °C, 7 days aged condition. (a) Niobium concentration profile; ±1 standard error bars are shown every 25 nm. (b) Experimental, LBM-fit, and binomial frequency distributions of the niobium concentrations; note that the experimental and LBM curves lie on top of one another. The LBM-fit niobium concentrations of the hypothetical coexisting phases were the average (15.4) + 2.4 and −1.6% Nb.

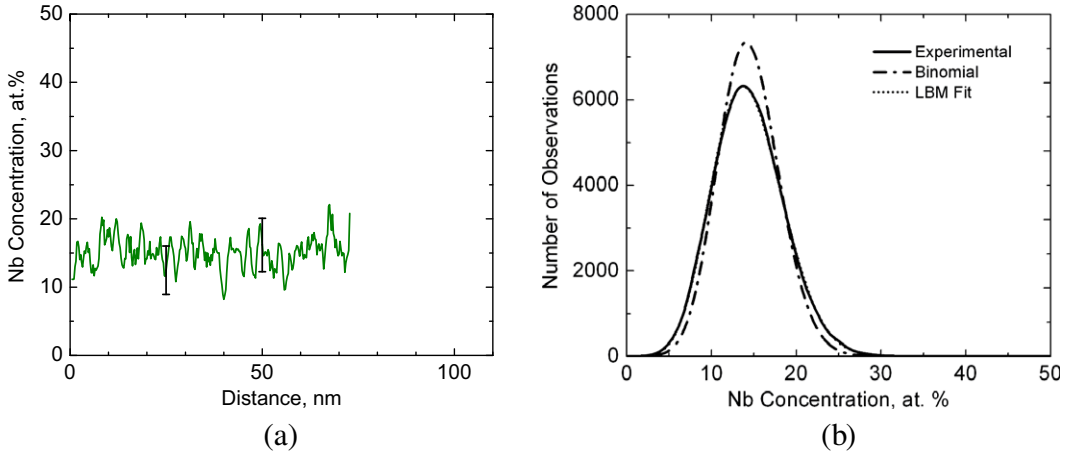

Fig. 7. APT results for the 200 °C, 70 days aged condition. (a) Niobium concentration profile; ±1 standard error bars are shown every 25 nm. (b) Experimental, LBM-fit, and binomial frequency distributions of the niobium concentrations; note that the experimental and LBM curves lie on top of one another. The LBM-fit niobium concentrations of the hypothetical coexisting phases were the average (14.4) + 2.2 and −1.6% Nb.

3.5. Atom probe tomography: quenched and aged at 200 °C

Specimens aged for 2 h, 16 h, 7 days, and 70 days at 200 °C were examined with the atom probe. Results from the 7 and 70 days aging conditions are considered representative of this series, and are provided in Figs. 6 and 7. The niobium concentration profiles in Figs. 6a and 7a are similar to that obtained for the AQ condition (Fig. 3a), and surprisingly do not differ substantially from each other. The apparent wavelength cannot be readily estimated from these plots, but appears to be <3 nm. Concentration profiles (not shown) were also obtained from three mutually orthogonal directions plus a randomly-selected direction for the 2 and 16 h aged conditions to check for preferred orientation growth associated with elastic accommodation, which is anticipated for a non-isotropic spinodal mechanism. No such patterning was observed, as similar niobium concentration profiles were obtained for each of the different orientations.

Experimental, binomial, and LBM frequency distributions for the 7 and 70 days aging conditions are shown in Figs. 6b and 7b. The solute concentrations for the coexisting hypothetical phases determined from the LBM method for these conditions are comparable to those obtained for the AQ condition, indicating that little change in the niobium distribution took place at 200 °C.

4. Discussion

4.1. Segregation to defects

Given the large number (∼10) of atom maps collected and analyzed in this study, the lack of noticeable patterns of niobium or substitutional impurity atom enrichment or depletion associated with twin boundaries is remarkable. This indicates that niobium or impurity atom segregation or precipitation at twin boundaries may not be responsible for age–hardening at $T \leqslant 300$ °C, contrary to suggestions made in previous studies [16,21,28]. The conspicuous absence of C, N, or O atoms in the APT analyses confirms that these elements were probably sequestered in inclusion phases prior to the solutionizing and aging treatments, and therefore do not contribute to age–hardening via segregation to twins.

4.2. Clustering and phase separation

Measurement of the degree of phase separation as a function of aging condition is of prime interest to this study. In this context, it is useful to consider the atom probe study on U–14% Nb by Beverini [22,36]; 350 °C data from this work were analyzed by Hetherington et al. [35] using the LBM method. A summary of selected results from their work, in addition to the results obtained from

Table 2
LBM best fit results of U–13% Nb or U–15% Nb aged at 200, 300, or 350 °C. The U–15% Nb results are from Hetherington et al. [35].

Nb in bulk alloy (at.%)	Aging temperature (°C)	Aging time	$\Delta c = \lvert\mu_2 - \mu\rvert$ (at.%)	σ (at.%)	χ^2	Degrees of freedom
13	–	AQ	3.0	1.0	29.1	30
13	200	2 h	3.3	0.7	41.2	29
13	200	2 h	3.5	0.2	44.9	29
13	200	2 h	3.6	1.3	56.5	30
13	200	16 h	3.6	0.7	54.1	29
13	200	16 h	3.3	0.1	22.4	29
13	200	16 h	3.5	1.1	141.3	32
13	200	7 days	4.0	1.0	79.0	32
13	200	70 days	3.8	1.0	41.0	30
13	200	70 days	4.2	1.0	57.8	30
13	300	70 days	12.8	4.0	1329.9	45
13	300	70 days	13.8	4.0	7982.6	46
15	350	3 h	11	3.0	10.4	17
15	350	5 h	9	3.0	13.3	19
15	350	6 h	15	3.0	20.1	27
15	350	7 h	16	5.0	12.7	27

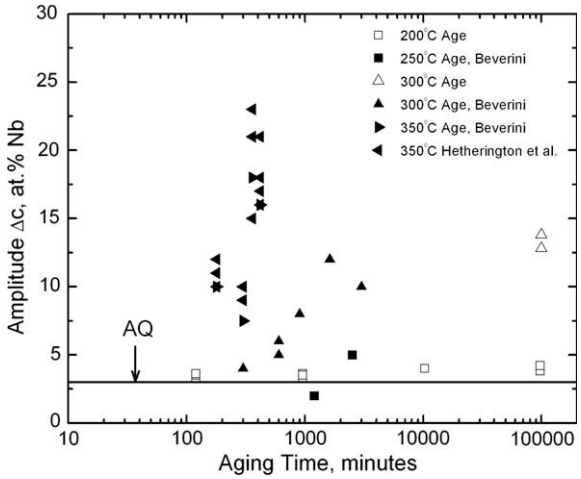

Fig. 8. Niobium redistribution amplitude $\Delta c = |\mu_2 - \mu_1|$ versus aging time at 200, 250, 300, or 350 °C for times up to 70 days. LBM amplitude/aging time combinations from Beverini [36] and Hetherington et al. [35] are also provided.

this study, is provided in Table 2. The block size used for the data in Table 2 is 100 atoms, although Hetherington et al. reported that their analysis results were largely independent of block size [35]. The difference between μ_2 and μ_1, indicative of the composition difference between the coexisting phases, generally increases with increasing aging time and temperature. The χ^2 values in Table 2 reflect the probability of fitting $|\mu_2 - \mu_1| = \Delta c$ to the experimental data. Hetherington et al. concluded that spinodal decomposition at 350 °C was possible, given the good agreement with the LBM analysis [35], although it is noted here that the LBM method provides solute concentrations of coexisting phases, regardless of the mechanism of phase separation, and thus would also be applicable to phase separation by mechanisms other than spinodal decomposition.

A summary of amplitude (Δc) versus aging time is provided in Fig. 8 that includes LBM analysis results from the current study, in addition to similar results from Hetherington et al. and Beverini [35,36]. The LBM Δc amplitude values generally increase with increasing time and temperature. Importantly, the Δc values obtained for the AQ, 200 °C, and 250 °C conditions do not differ substantially, even after long times (200 °C for 70 days), suggesting that no significant solute partitioning or segregation is occurring on these timescales at 200 and 250 °C.

The current results show that phase separation into niobium-depleted and enriched regions occurs during aging at 300 °C for 70 days. Regardless of how the niobium is arranged in the enriched and depleted regions (i.e., same-phase cluster/spinodal region or second-phase precipitate), the small 6–8 nm spacing observed in the 300 °C, 70 days aging condition is consistent with the observed level of strengthening. Evidence of significant niobium redistribution is not evident after aging at 200 °C for times up to 70 days, even though substantial changes in hardness, strength, and ductility are observed (Fig. 2). An alternate strengthening mechanism based on niobium or impurity atom segregation to twin interfaces [21,22,24,28] might also provide a reasonable explanation for this hardening, but was not supported since no segregation patterns were detected at either aging temperature.

Table 3
Calculated diffusion distances for Nb in U (Q_{diff} = 136.4 kJ/mol).

T (°C)	Time t	$2\sqrt{Dt}$ (nm)	
		$D_0 = 1.38 \times 10^{-8}$ m^2/s	$D_0 = 7.2 \times 10^{-12}$ m^2/s
200	120 min (=2 h)	0.59	0.013
200	100,000 min (≈70 days)	17	0.39
300	120 min (=2 h)	12	0.28
300	100,000 min (≈70 days)	350	**8.0**

Consideration of the relative diffusion rates at 200 versus 300 °C can provide a check into the likelihood of diffusion-driven phase-separation. Phenomenological studies of hardening in this temperature regime for the same alloy have yielded activation energies in the range of 121–138 kJ/mol for changes in second yield strength and tensile elongation to failure [24]. These are comparable to the 136.4 kJ/mol activation energy for volume diffusion (Q_{diff}) of Nb in γ-U determined in the 700–1000 °C range [31]. Calculations of characteristic diffusion length $2\sqrt{Dt}$ values for 2 h and ~70 days at 200 and 300 °C, based on the extrapolated diffusivity using the same values of Q_{diff} and the pre-exponential (D_0), are provided in Table 3. Note that the value for 300 °C, 70 days is much larger than 6–8 nm, the apparent separation distance of the Nb rich regions observed experimentally. By adjusting D_0 to match the observed separation at 300 °C while holding Q constant (based on the observation that this value is consistent with the experimentally observed activation energy for hardening), the expected diffusion distances at 200 °C can be recalculated (right-most column). These values are 0.013 and 0.39 nm for 2 h and ~70 days, respectively, well below the resolution of the LEAP instrument and, in the case of 2 h, less than the atomic radius. This would suggest that a classical diffusion-driven phase-separation mechanism is highly unlikely to be responsible for the observed property changes at 200 °C, particularly for shorter times.

Therefore, consideration of alternate aging mechanisms may be warranted in light of these findings. One example may be twin interfacial structures rearranging into lower energy configurations by viscous glide, climb, or ledge/step migration, especially at short or intermediate times at low temperatures. Also, electronic instabilities have been observed in pure α-uranium in the form of charge-density waves [37]. Related phenomena in this alloy could result in incommensurate atomic movements on an extremely fine scale (⩽3 nm), resulting in strengthening.

4.3. Assessment of proposed spinodal and ordering mechanisms

Both early and more recent studies have suggested spinodal decomposition [2,16,22,26,27] and/or chemical ordering [26,27] as the specific mechanism responsible for low-temperature age–hardening in U–14% Nb alloys. As discussed previously, broadening of the frequency distribution with respect to the binomial distribution is consistent with clustering or phase separation, whereas narrowing of the frequency distribution is associated with ordering. The fact that broadening of the distribution with respect to the binomial is observed in all of the conditions examined (even the AQ condition) leads to the conclusion that ordering is not viable as an aging mechanism in this system. The other two major phase separation mechanisms – spinodal and nucleation-and-growth (N&G) – are considered in the following.

It is difficult to prove a spinodal mechanism in any alloy system because the decomposition morphology alone is equivocal: the final microstructure, for example, one that is percolated [38], can look exactly like one formed via N&G [39]. Direct proof of a spinodal mechanism can be obtained from time-series measurements of concentration fluctuation amplitudes, which for example were performed via small-angle X-ray scattering in Al–Zn [40], and more recently by 3DAP in Fe–Cr [41–43]. The aging times examined in previous U–Nb aging studies [22,35,36] as well as the present one do not span a sufficiently long period of aging time to give direct evidence for or against a spinodal mechanism. In light of this lack of direct data, consideration will be made of thermodynamic and other arguments to assess the likelihood of a spinodal mechanism in binary uranium alloys with 13–14% Nb aged at ⩽300 °C.

Table 4
Ancillary data used in calculation of the U–Nb γ phase miscibility gap and spinodal curves.

Parameter	Symbol	Value	Comments/reference
Elastic (Young's) modulus	E	68.9 (GPa)	This value is the same for both U–14.7% Nb and U–19.0% Nb [28]
Poisson's ratio	ν	0.35	U–14.7% Nb value [28]
Linear coefficient of thermal expansion	CTE	1.454×10^{-5} (K^{-1})	From U–13.2% Nb dilatometry [24]
Nb-dependence of lattice parameter	η	−0.074 (at. fr. Nb)$^{-1}$	Quadratic fit from [48] with CTE as above
Molar volume	V_m	1.2798×10^{-5} (m^3 mol^{-1})	Evaluated at U–14% Nb using [48] quadratic fit
Gibbs free energy reference state for pure U	$(G - H_{SER})_U$	$-752.767 + 131.5381T - 27.5152T \ln T + 8.35595 \times 10^{-3}T^2 + 9.67907 \times 10^{-7}T^3 + 204611T^{-1}$ (J mol^{-1})	Valid over 298–1049 K; temperature in formula is in Kelvin [49]
		$-4698.365 + 202.685635T - 38.2836T \ln T$ (J mol^{-1})	Valid over 1049–3000 K; temperature in formula is in Kelvin [49]
Gibbs free energy reference state for pure Nb	$(G - H_{SER})_{Nb}$	$-8519.353 + 142.045475T - 26.4711T \ln T + 2.03475 \times 10^{-4}T^2 - 3.5012 \times 10^{-7}T^3 + 93399T^{-1}$ (J mol^{-1})	Valid over 298–2750 K; temperature in formula is in Kelvin [49]
Subregular solution parameters	A	16,050 (J mol^{-1})	
	B	3.78954 (J mol^{-1} K^{-1})	

Whether spinodal decomposition is a viable mechanism depends in part on the phase in which the material is aged. In principle, spinodal decomposition is possible in the γ phase, by virtue of its miscibility gap, seen in Fig. 1. No data exist that would indicate a miscibility gap in α′ or α″. In fact, negligible niobium solubility in the equilibrium α phase argues strongly against a miscibility gap in any of these α-related metastable phases. Prior to aging the U–13.2% Nb microstructure is α″; reverse martensitic transformation(s) can take place upon heating to the aging temperature. Dilatometry measurements of the austenite-start (A_s) and -finish (A_f) temperatures for this alloy composition and a ~40 K/s heating rate are 180±20 and 209±17 °C, respectively, for the $\alpha'' \rightarrow \gamma^0$ transformation and 310 ± 28 and 391 ± 2 °C, respectively, for the $\gamma^0 \rightarrow \gamma$ transformation [24]. It is noted that these temperatures may be heating rate dependent [29]. For example, heating (typically within 30 min) of U–13% Nb to 300 °C in a vacuum furnace during an in situ neutron diffraction experiment indicated the formation of γ^0 on heating, followed by the presence of both α″ and γ^0 during a 36 h hold [30]. Formation of the γ^0 phase was not observed at 200 °C during the same study. Slower heating in a vacuum furnace to 325 °C over a period of 15 h resulted in the presence of only α″ [30]. The γ^0 phase was not formed during slow heating, even at a temperature ~100 °C above the nominal A_f. The heating rate in the current study is comparable to the faster of the two neutron experiments. No significant transformation to γ^0 is expected during aging at 200 °C, so spinodal decomposition in α″ (or α′) is unlikely on the arguments made previously. The sequence $\alpha'' \rightarrow \alpha'$ (niobium depleted) + γ^0/γ (niobium enriched) with further evolution towards $\alpha + \gamma_2$ is anticipated, if the diffusion kinetics are sufficient.

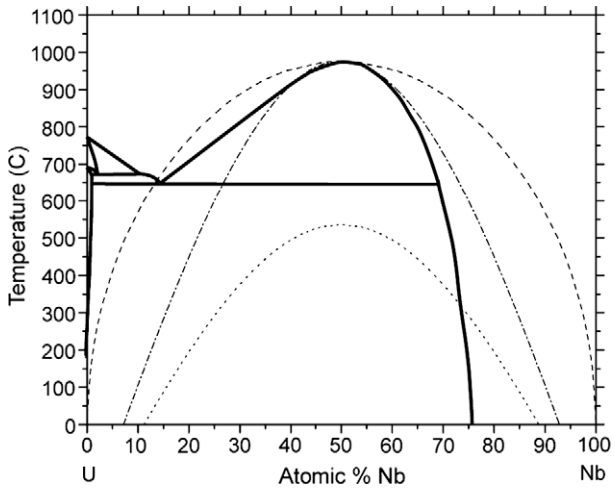

Fig. 9. Calculated chemical miscibility gap (dashed line), chemical spinodal (dot-dash line), and coherent spinodal (dotted line). The solid-state phase boundaries according to Koike et al. [15] (see Fig. 1) are superimposed as bold solid lines.

At 300 °C the sequence $\alpha'' \rightarrow \gamma^0/\gamma \rightarrow \alpha''/\alpha'$ (niobium lean) + γ (niobium enriched) $\rightarrow \alpha + \gamma_2$, is expected. However, spinodal decomposition of the γ^0/γ must also be considered. The γ^0 phase is a slight tetragonal distortion of γ, and therefore might be expected to behave similarly with regards to the analysis of the γ phase miscibility gap described below.

A simple thermodynamic model was developed to calculate the chemical miscibility gap and spinodal lines for the γ phase of the U–Nb system. The molar Gibbs free energy of the γ phase was modeled with a subregular solution:

$$G = (1-x)(G - H_{SER})_U + x(G - H_{SER})_{Nb} + (A + BT)x(1-x) + RT[x \ln x + (1-x)\ln(1-x)] \quad (1)$$

The composition x is the niobium mole fraction, R is the gas constant, T is the absolute temperature, and A and B are adjustable parameters. These parameters and other ancillary data are listed in Table 4. The first two terms in the equation are the standard states of the pure elements. The subregular solution parameters A and B were adjusted to give a critical temperature T_c = 977 °C [44] and to have the Nb-lean portion of the miscibility gap intersect the 647 °C monotectoid isotherm at the assessed value of x = 0.133 [15]. The calculated miscibility gap (Fig. 9) is considerably wider than the experimental γ miscibility gap [15], indicating that a more sophisticated solution thermodynamic model is required to faithfully match experiment. Nonetheless, since this calculation likely overstates the bounds of the miscibility gap and spinodal lines, it gives a liberal assessment of the likelihood of an actual spinodal decomposition reaction in alloys of x = 0.13–0.14 aged at temperatures ⩽300 °C.

The spinodal points in (x, T)-space are defined where the G–x curve inflects [45] and bound the (x, T)-space where Nb concentration fluctuations will spontaneously amplify in the absence of any discrete nucleation event to give spinodal decomposition. For the chemical spinodal, this is defined as

$$\partial^2 G/\partial x^2 \leqslant 0. \quad (2)$$

This was evaluated numerically, and is shown as the dot-dash line in Fig. 9. The energy sink associated with elastic strain energy will depress the spinodal to lower temperatures. This effective or "coherent" spinodal curve is defined by

$$\partial^2 G/\partial x^2 + 2\eta^2 Y V_m \leqslant 0, \quad (3)$$

where V_m is the molar volume, η is the lattice parameter variation with composition $(1/a)\,da/dx$ and Y is the effective elastic modulus, equal to $E/(1-\nu)$ in an isotropic solid [45]. Values of these parameters were taken from U–Nb literature and are listed in Table 4.

The calculated coherent spinodal in Fig. 9 is depressed by ~200–400 °C with respect to the chemical spinodal, highlighting the significant influence of strain energy in the U–Nb γ phase. This is consistent with the results of a companion X-ray diffraction study on the same alloy that indicated large coherency strains in the aged microstructure [25]. With this significant level of strain energy (somewhat larger than that found in a study of the related Nb–Zr monotectoid system [46]), any spinodal modulations would be expected to be patterned along either {1 0 0} or {1 1 1} planes [47]. Characteristic patterning of this type was not observed in the 3D isoconcentration surface renderings of the APT data in this study (e.g., Fig. 5), although it is noted that APT does not provide crystallographic information. The isoconcentration surfaces instead appeared roughly equiaxed, which provides indirect evidence against a directionally-specific spinodal mechanism.

Calculated coherent spinodal points (x, T) at temperatures of interest include: (0.202, 200 °C) and (0.254, 300 °C). Both of these thresholds are well beyond of the $x = 0.13$–0.14 compositions of interest. Given that the calculated chemical spinodal region is likely an overestimate of the γ phase, and is almost certainly larger than any hypothetical spinodal in the α'' or γ^0 phases, it is concluded that a spinodal mechanism is unlikely at any temperature for alloys in the $x = 0.13$–0.14 range.

5. Conclusions

Atom probe tomography examination of aged U–13% Nb was performed to determine the low-temperature age–hardening mechanism(s) in the U–Nb system. The enhanced capabilities of current APT instrumentation enabled an improved level of discrimination between various proposed aging mechanisms premised on chemical redistribution. The following conclusions were obtained:

(1) Increasing strength and hardness are accompanied by significant ductility loss after aging at 200 or 300 °C for times up to 70 days.
(2) Segregation of niobium or impurity atoms to twin interfaces is not apparent, making this hardening mechanism unlikely.
(3) Phase separation into regions of high and low niobium concentration occurs after aging at 300 °C for 70 days, with a length scale of 6–8 nm.
(4) Very subtle niobium concentration changes are observed after aging at 200 °C, suggesting that consideration of aging mechanisms other than those involving more classical niobium redistribution may be warranted at low temperatures.
(5) Aging mechanisms involving spinodal and/or ordering are not supported by the atom probe results. Theoretical analysis of spinodal decomposition in U–Nb also indicates that it is unlikely in alloys containing 13–14 wt.% Nb aged at temperatures $\leqslant$300 °C.

Acknowledgements

LANL support was provided by the US Department of Energy (Contract Number DE-AC52-06NA25396) and the G.T. Seaborg Institute for Transactinium Science. Research at the Oak Ridge National Laboratory SHaRE User Facility was sponsored by the Office of Science, Office of Basic Energy Sciences, Scientific User Facilities Division, US Department of Energy with UT-Battelle, LLC. We thank J.A. Balog for machining the atom probe specimen blanks, T. Tucker and W.L. Hults for performing the heat treatments, and M.F. Lopez for performing the tensile testing. A.M. Kelly, R.S. Casey, and R.T. Forsyth are gratefully acknowledged for the metallography and hardness testing. Helpful discussions regarding this work with K.H. Eckelmeyer and J.P. Hirth are also greatly appreciated.

References

[1] K.H. Eckelmeyer, Uranium and uranium alloys, ASM Handbook, vol. 2, ASM, Materials Park, OH, 1990, p. 670.
[2] K.H. Eckelmeyer, A.D. Romig Jr., L.J. Weirick, Metall. Trans. A 15A (1984) 1319.
[3] M. Anagnostidis, M. Colombie, H. Monti, J. Nucl. Mater. 11 (1964) 67.
[4] K. Tangri, D.K. Chaudhuri, C.N. Rao, J. Nucl. Mater. 15 (1965) 278.
[5] R.D. Field, D.J. Thoma, P.S. Dunn, D.W. Brown, C.M. Cady, Philos. Mag. A 81 (2001) 1691.
[6] H.L. Yakel, J. Nucl. Mater. 33 (1969) 286.
[7] K. Tangri, G.I. Williams, J. Nucl. Mater. 4 (1961) 226.
[8] B.A. Hatt, J. Nucl. Mater. 19 (1966) 133.
[9] R.A. Vandermeer, J.C. Ogle, W.B. Snyder Jr., Scr. Metall. 12 (1978) 243.
[10] R.A. Vandermeer, J.C. Ogle, W.G. Northcutt, Metall. Trans. A 12A (1981) 733.
[11] R.A. Vandermeer, D.A. Carpenter, W.G. Northcutt, J.C. Ogle, Effects of tensile deformation on the strain memory behavior of uranium–niobium alpha martensite, in: H.I. Aaronson, D.E. Laughlin, R.F. Sekerka, C.M. Wayman (Eds.), Proc. Int. Conf. Solid–Solid Phase Transformations, TMS-AIME, Warrendale, PA, 1982, p. 1299.
[12] R.D. Field, D.W. Brown, D.J. Thoma, Philos. Mag. 85 (2005) 2593.
[13] R.D. Field, D.W. Brown, D.J. Thoma, Shape memory behavior in U–Nb alloys, in: J.M. Howe, D.E. Laughlin, J.K. Lee, U. Dahmen, W.A. Soffa (Eds.), International Conference on Solid–Solid Phase Transformations in Inorganic Materials (PTM 2005), vol. 2. TMS, Warrendale, PA, 2005, p. 227.
[14] A.J. Clarke, R.D. Field, R.J. McCabe, C.M. Cady, R.E. Hackenberg, D.J. Thoma, Acta Mater. 56 (2008) 2638.
[15] J. Koike, M.E. Kassner, R.E. Tate, R.S. Rosen, J. Phase, Equilibria 19 (1998) 253.
[16] R.J. Jackson, Isothermal Transformations of Uranium-13 Atomic Percent Niobium, Report RFP-1609, Rocky Flats Plant, Golden, CO, 1971.
[17] C. D'Amato, F.S. Saraceno, T.B. Wilson, Nucl. Mater. 12 (1964) 291.
[18] R.J. Jackson, R.P. Brugger, D.V. Miley, Tensile Properties of Gamma Quenched and Aged Uranium-Rich Niobium Alloys, Report RFP-933, Rocky Flats Plant, Golden, CO, 1967.
[19] R.J. Jackson, D.V. Miley, Trans. ASM 61 (1968) 336.
[20] B. Djuric, J. Nucl. Mater. 44 (1972) 207.
[21] K.H. Eckelmeyer, Aging phenomena in dilute uranium alloys, in: J.J. Burke, D.A. Colling, A.E. Gorum, J. Greenspan (Eds.), Physical Metallurgy of Uranium Alloys, Brook Hill, Chestnut Hill, MA, 1976, p. 463.
[22] G. Beverini, D.V. Edmonds, J. Phys. (Coll.) 50-C8 (1989) 429.
[23] R.J. Jackson, J.F. Boland, Mechanical Properties of Uranium-Base Niobium Alloys, Report RFP-1703, Rocky Flats Plant, Golden, CO, 1971.
[24] R.E. Hackenberg, D.W. Brown, A.J. Clarke, L.B. Dauelsberg, R.D. Field, W.L. Hults, A.M. Kelly, M.F. Lopez, D.F. Teter, D.J. Thoma, T.J. Tucker, C.J. Vigil, H.M. Volz, U–Nb Aging Final Report, Report LA-14327, Los Alamos National Laboratory, Los Alamos, NM, 2007.
[25] H.M. Volz, R.E. Hackenberg, A.M. Kelly, W.L. Hults, A.C. Lawson, R.D. Field, D.F. Teter, D.J. Thoma, J. Alloys Comp. 444–445 (2007) 217.
[26] L.L. Hsiung, Spinodal decomposition and ordering transformation in U–6 wt% Nb, in: J.M. Howe, D.E. Laughlin, J.K. Lee, U. Dahmen, W.A. Soffa (Eds.), International Conference on Solid–Solid Phase Transformations in Inorganic Materials (PTM 2005), vol. 1. TMS, Warrendale, PA, 2005, p. 209.
[27] J. Zhou, L.M. Hsiung, J. Mater. Res. 21 (2006) 904.
[28] R.J. Jackson, Elastic, plastic and strength properties of U–Nb and U–Nb–Zr alloys, in: J.J. Burke, D.A. Colling, A.E. Gorum, J. Greenspan (Eds.), Physical Metallurgy of Uranium Alloys, Brook Hill, Chestnut Hill, MA, 1976, p. 611.
[29] R.A. Vandermeer, Acta Metall. 28 (1980) 383.
[30] D.W. Brown, Unpublished Research, Los Alamos National Laboratory, Los Alamos, NM, 2005.
[31] N.L. Peterson, R.E. Ogilvie, Trans. TMS-AIME 227 (1963) 1083.
[32] M.K. Miller, Atom Probe Tomography Analysis at the Atomic Level, Kluwer Academic/Plenum, New York, 2000.
[33] R.E. Hackenberg, R.M. Aikin, Jr., J.A. Balog, B.L. Bingham, R. Casey, A. Casteel, I. Cordova, R. Forsyth, F.G. Garcia, D. Guidry, D.L. Hammon, W.L. Hults, D.R. Korzekwa, A.M. Kelly, M.W. Koby, K.A. Lao, J.C. Lashley, M.F. Lopez, R. McCabe, D.E. Nye, P.A. Papin, S.W. Quintana, J.L. Smith, D.F. Teter, D.J. Thoma, T. Tucker, P.K. Tubesing, R.R. Trujillo, C.J. Vigil, H.M. Volz, Synthesis and Characterization of Nonbanded U–Nb Plate Material, Report LA-14316, Los Alamos National Laboratory, Los Alamos, NM, 2007.
[34] J.S. Langer, M. Bar-On, H.D. Miller, Phys. Rev. A 11 (1975) 1417.
[35] M.G. Hetherington, J.M. Hyde, M.K. Miller, G.D.W. Smith, Surf. Sci. 246 (1991) 304.
[36] G. Beverini, Phase Transformations in Binary Uranium Alloys, PhD Dissertation, University of Oxford, Oxford, 1991.
[37] C.H. Chen, G.H. Lander, Phys. Rev. Lett. 57 (1986) 110.
[38] M.K. Miller, in: G.W. Lorimer (Ed.), Phase Transformations '87, Institute of Metals, London, 1988, p. 39.
[39] K. Binder, P. Fratzl, Spinodal decomposition, in: G. Kostorz (Ed.), Phase Transformations in Materials, Wiley-VCH, Weinheim, 2001, p. 409.
[40] K.B. Rundman, J.E. Hilliard, Acta Metall. 15 (1967) 1035.
[41] M.K. Miller, J.M. Hyde, M.G. Hetherington, A. Cerezo, G.D.W. Smith, C.M. Elliott, Acta Metall. Mater. 43 (1995) 3385.
[42] J.M. Hyde, M.K. Miller, M.G. Hetherington, A. Cerezo, G.D.W. Smith, C.M. Elliott, Acta Metall. Mater. 43 (1995) 3403.

[43] J.M. Hyde, M.K. Miller, M.G. Hetherington, A. Cerezo, G.D.W. Smith, C.M. Elliott, Acta Metall. Mater. 43 (1995) 3415.
[44] ASM Alloy Phase Diagrams Center, in: P. Villars (Editor-in-chief), H. Okamoto, K. Cenzual (section Eds.), ASM International, Materials Park, OH, 2006.
[45] J.E. Hilliard, Spinodal decomposition, in: Phase Transformations, ASM, Metals Park, OH, 1970, p. 497.
[46] P.E.J. Flewitt, Acta Metall. 22 (1974) 47.
[47] J.W. Cahn, Acta Metall. 10 (1962) 179.
[48] P.C.L. Pfeil, J.D. Browne, G.K. Williamson, J. Instrum. Met. 87 (1958–1959) 204 (London).
[49] A.T. Dinsdale, Calphad 15 (1991) 317.